Clin Orthop Relat Res (2015) 473:2885–2897
DOI 10.1007/s11999-015-4312-z

Clinical Orthopaedics and Related Research®
A Publication of The Association of Bone and Joint Surgeons®

SYMPOSIUM: RESEARCH ADVANCES AFTER A DECADE OF WAR

Hydrogel-based Delivery of rhBMP-2 Improves Healing of Large Bone Defects Compared With Autograft

Laxminarayanan Krishnan PhD, Lauren B. Priddy MS, Camden Esancy BS, Mon-Tzu Alice Li PhD, Hazel Y. Stevens BS, Xi Jiang BS, Lisa Tran MD, David W. Rowe PhD, Robert E. Guldberg PhD

Published online: 28 April 2015

Abstract

Background Autologous bone grafting remains the gold standard in the treatment of large bone defects but is limited by tissue availability and donor site morbidity. Recombinant human bone morphogenetic protein-2 (rhBMP-2), delivered with a collagen sponge, is clinically used to treat large bone defects and complications such as delayed healing or non-union. For the same dose of rhBMP-2, we have shown that a hybrid nanofiber mesh-alginate (NMA-rhBMP-2) delivery system provides longer-term release and increases functional bone regeneration in critically sized rat femoral bone defects compared with a collagen sponge. However, no comparisons of healing efficiencies have been made thus far between this hybrid delivery system and the gold standard of using autograft.

Questions/purposes We compared the efficacy of the NMA-rhBMP-2 hybrid delivery system to morselized autograft and hypothesized that the functional regeneration of large bone defects observed with sustained BMP delivery would be at least comparable to autograft treatment as measured by total bone volume and ex vivo mechanical properties.

Methods Bilateral critically sized femoral bone defects in rats were treated with either live autograft or with the NMA-rhBMP-2 hybrid delivery system such that each animal received one treatment per leg. Healing was monitored by radiography and histology at 2, 4, 8, and 12 weeks. Defects were evaluated for bone formation by longitudinal micro-CT scans over 12 weeks (n = 14 per group). The bone volume, bone density, and the total new bone formed beyond 2 weeks within the defect were calculated from micro-CT reconstructions and values compared for the 2-, 4-, 8-, and 12-week scans within and across the two treatment groups. Two animals were used for bone labeling with subcutaneously injected dyes at 4, 8, and 12 weeks followed by histology at 12 weeks to

Funding was received from the Armed Forces Institute of Regenerative Medicine (REG).
All ICMJE Conflict of Interest Forms for authors and *Clinical Orthopaedics and Related Research*® editors and board members are on file with the publication and can be viewed on request.
Clinical Orthopaedics and Related Research® neither advocates nor endorses the use of any treatment, drug, or device. Readers are encouraged to always seek additional information, including FDA-approval status, of any drug or device prior to clinical use.
Each author certifies that his or her institution approved the animal protocol for this investigation and that all investigations were conducted in conformity with ethical principles of research.
This work was performed at the Parker H. Petit Institute for Bioengineering & Bioscience, Georgia Institute of Technology, Atlanta, GA, USA; and the University of Connecticut Health Center, Farmington, CT, USA.

L. Krishnan, L. B. Priddy, C. Esancy, M.-T. A. Li, H. Y. Stevens, R. E. Guldberg (✉)
Parker H. Petit Institute for Bioengineering & Bioscience, Georgia Institute of Technology, 315 Ferst Drive, Atlanta, GA 30332-0363, USA
e-mail: robert.guldberg@me.gatech.edu

L. B. Priddy, M.-T. A. Li, R. E. Guldberg
Wallace H. Coulter Department of Biomedical Engineering, Georgia Institute of Technology & Emory University, Atlanta, GA, USA

H. Y. Stevens, R. E. Guldberg
George W. Woodruff School of Mechanical Engineering, Georgia Institute of Technology, Atlanta, GA, USA

M.-T. A. Li, L. Tran
Emory University, Atlanta, GA, USA

X. Jiang, D. W. Rowe
University of Connecticut Health Center, Farmington, CT, USA

identify incremental new bone formation. Functional recovery was measured by ex vivo biomechanical testing (n = 9 per group). Maximum torque and torsional stiffness calculated from torsion testing of the femurs at 12 weeks were compared between the two groups.

Results The NMA-rhBMP-2 hybrid delivery system resulted in greater bone formation and improved biomechanical properties compared with autograft at 12 weeks. Comparing new bone volume within each group, the NMA-rhBMP-2-treated group had higher volume ($p < 0.001$) at 12 weeks (72.59 ± 18.34 mm^3) compared with 8 weeks (54.90 ± 16.14) and 4 weeks (14.22 ± 9.59). The new bone volume was also higher at 8 weeks compared with 4 weeks ($p < 0.001$). The autograft group showed higher ($p < 0.05$) new bone volume at 8 weeks (11.19 ± 8.59 mm^3) and 12 weeks (14.64 ± 10.36) compared with 4 weeks (5.15 ± 4.90). Between groups, the NMA-rhBMP-2-treated group had higher ($p < 0.001$) new bone volume than the autograft group at both 8 and 12 weeks. Local mineralized matrix density in the NMA-rhBMP-2-treated group was lower than that of the autograft group at all time points ($p < 0.001$). Presence of nuclei within the lacunae of the autograft and early appositional bone formation seen in representative histology sections suggested that the bone grafts remained viable and were functionally engrafted within the defect. The bone label distribution from representative sections also revealed more diffuse mineralization in the defect in the NMA-rhBMP-2-treated group, whereas more localized distribution of new mineral was seen at the edges of the graft pieces in the autograft group. The NMA-rhBMP-2-treated group also revealed higher torsional stiffness (0.042 ± 0.019 versus 0.020 ± 0.022 N-m/°; $p = 0.037$) and higher maximum torque (0.270 ± 0.108 versus 0.125 ± 0.137 N-m; $p = 0.024$) compared with autograft.

Conclusions The NMA-rhBMP-2 hybrid delivery system improved bone formation and restoration of biomechanical function of rat segmental bone defects compared with autograft treatment.

Clinical Relevance Delivery systems that allow prolonged availability of BMP may provide an effective clinical alternative to autograft treatment for repair of segmental bone defects. Future studies in a large animal model comparing mixed cortical-trabecular autograft and the NMA-rhBMP-2 hybrid delivery system are the next step toward clinical translation of this approach.

Introduction

Large segmental bone defects result from trauma, tumor resection, skeletal reconstructions, and infections. Despite the endogenous regenerative capacity of bone, defects that are critically sized do not heal spontaneously and require therapeutic augmentation. Bone grafting has historically constituted the main therapeutic intervention in these volume-filling applications. Autograft, surgically obtained from the patient, has persisted as the gold standard of treatment but has also been associated with a multitude of complications at the donor site, limited availability, and variation in ultimate outcomes (eg, eventual nonunion in some cases) [25, 45]. Use of different harvest sites or combined use of cortical grafts with limited amounts of cancellous bone may not be sufficient to overcome these challenges and thus motivates continued investigation of alternative treatment strategies [17, 19, 32, 45].

Allograft, demineralized bone matrices, biomaterial scaffolds, and the highly potent osteoinductive factor bone morphogenetic protein (BMP) are common alternatives to autograft. Allograft has reduced osteoinductive potential and slower healing, whereas demineralized scaffolds lack structural stability [1, 13, 19, 25]. The widespread use of recombinant human BMP-2 (rhBMP-2) highlights its capability to augment large segmental bone defect repair, especially in the context of animal studies, with BMP-2 supplementation showing improved healing compared with allograft and ceramic fillers [25, 46]. Concerns about BMP-2 side effects, optimal delivery scaffolds, and BMP-2 release kinetics notwithstanding, rhBMP-2 delivered in an absorbable collagen sponge (ACS-rhBMP-2) has become a popular clinical alternative to bone grafting in the United States while tunable delivery systems with tailored BMP release kinetics are sought [28, 47].

Alginate hydrogels modified through the addition of arginine-glycine-aspartic acid (RGD) to promote cell adhesion and gamma-irradiation to enhance degradation have been used for bone tissue engineering [2, 3, 36, 39]. We have previously observed higher mineral content and biomechanical properties in critically sized femoral segmental defects treated with a perforated nanofiber mesh enclosing RGD-alginate and rhBMP-2 (NMA-rhBMP-2) hybrid delivery system at equivalent doses and with advantageous rhBMP-2 release kinetics as compared with ACS-rhBMP-2 [8, 9, 27, 28]. However, its performance relative to autograft, the gold standard, is unknown.

Our goal in this study was therefore to compare healing with cortical autograft treatment to the NMA-rhBMP-2 hybrid delivery system. Our primary questions were (1) whether the NMA-rhBMP-2 group would produce quantitatively similar levels of bone mineral volume (BV) and bone mineral density (BD) to freshly harvested autograft; and if so, (2) whether the biomechanical properties of the healed bones would be different between treatments. Using vital bone labels [42] (fluorochromes binding the

mineralizing front of bone tissue) and histology, we also determined the quality and distribution of the regenerated bone.

Materials and Methods

Study Design

All animal procedures were approved by the Georgia Tech Institutional Animal Care and Use Committee. Bilateral critically sized segmental defects (8 mm length) [8, 34] were created in the middiaphysis of femora of 13-week-old female Sasco Sprague-Dawley rats (Charles River, Wilmington, MA, USA) after stabilization of each femur with a fixation plate (Fig. 1A). Animal age, gender, and strain were chosen for their size compatibility for longitudinal micro-CT analysis as established in previous studies with this model [8–10, 27, 28]. A porous electrospun polycaprolactone nanofiber mesh (NFM) sheet (12 × 19 mm) with 1-mm diameter perforations was preformed into a tube and positioned around the proximal and distal stumps of the femur such that it completely enclosed the defect space and spatially retained the delivered therapeutics within the defect space (Fig. 1B) [28]. The two treatments—autograft or NMA-rhBMP-2—were evaluated in the same animal with randomized allocation of treatment to the left or right limb for each group. The alginate treatment was always administered first to allow harvesting of both middiaphyseal regions, which were then combined to create the autograft implants for the contralateral defect. The muscles were sutured over the defect and the skin closed with wound clips. Animals were given a single injection of sustained-release buprenorphine (Wildlife Pharmaceuticals, Windsor, CO, USA) for analgesia. Unrestricted ambulation was allowed and the healing progress was observed over a 12-week period. Of 23 animals, one animal was euthanized on Day 0 to provide initial morselized bone graft morphology and one animal was noted to have an infection in the defect region on euthanasia at 12 weeks. All other surgeries and recovery in the study design (Fig. 1C) were considered uneventful. Samples were assigned for routine histology at four time points 2, 4, 8, and 12 weeks (n = 1–2). Two animals were assigned for sequential vital bone labeling at three time points (4, 8, and 12 weeks)

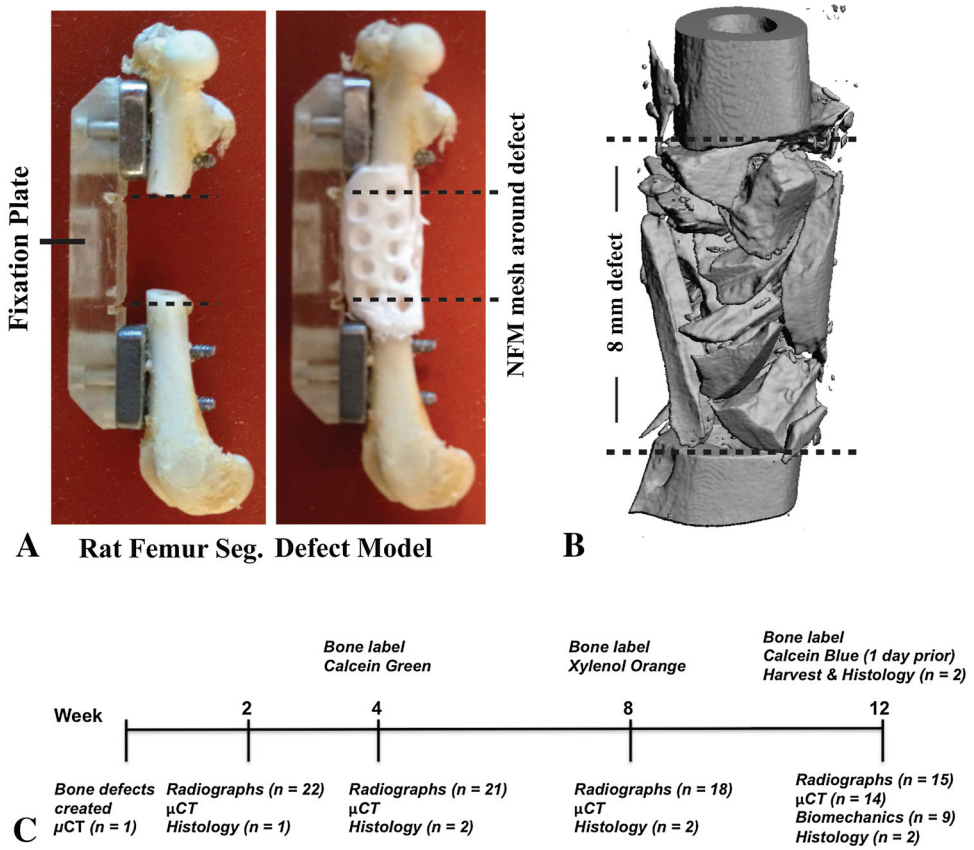

Fig. 1A–C (**A**) Rat femur with polysulfone stabilization plates showing the middiaphyseal defect, polysulfone fixation plate, and poly-caprolactone (PCL) nanofiber (NFM) mesh tube fitting around the proximal and distal stumps to enclose the defect space. (**B**) Three-dimensional reconstruction of the micro-CT image of an autograft treated sample showing the relative sizes of the cortical bone fragments. (**C**) A schematic showing the experiment design including interventions, outcome measures, and sample numbers.

followed by terminal fixation and cryoprocessing (12 weeks). Nine samples from each group were used for ex vivo biomechanical testing. For histological analyses, animals were anesthetized and the ascending aorta was catheterized through the left ventricle followed by perfusion fixation with 10% neutral-buffered formalin (Fisher Scientific, Pittsburgh, PA, USA). For mechanical testing, legs were harvested immediately after euthanasia by CO_2 inhalation, wrapped in saline-soaked gauze, and stored at −20 °C.

Therapeutics

Alginate Hydrogels (NMA-rhBMP-2)

Irradiated sodium alginate functionalized with RGD peptide sequences (FMC Biopolymer, NovaMatrix, Sandvik, Norway) was reconstituted in alpha-MEM (Gibco, Grand Island, NY, USA) to yield a 2% w/v alginate solution. Recombinant human bone morphogenetic protein (R&D Systems, Minneapolis, MN, USA) was suspended in 0.1% rat serum albumin (Sigma, St Louis, MO, USA) solution in 4 mM hydrochloric acid, and appropriate volumes were added to provide 5 µg of rhBMP-2 per 150 µL of the alginate solution. The alginate solution was gelled by vigorous mixing after the addition of calcium sulfate (0.21 g/mL, 25:1 ratio). All materials were aseptically prepared in a laminar flow hood, and the hydrogels were stored sterile overnight at 4 °C. During surgery, 150 µL of alginate hydrogel, kept on ice between uses, was injected into the defect space through the perforations in the NFM tube as previously established [8, 27, 34].

Autograft

The diaphyseal segments obtained from both the right and left femora were cleared of soft tissue, placed in saline until use, and manually minced (morselized) into smaller pieces in a sterile container using a bone cutter. The morselized pieces showed a large distribution in size (Fig. 1B) and were not characterized quantitatively. The cortical autograft pieces were used to completely fill the inside of the NFM tube, which was then placed around the ends of the bone stumps (Fig. 1B).

Radiological and Micro-CT Analysis of Bone Regeneration

Sequential radiographs were used to qualitatively assess defect bridging at 2, 4, 8, and 12 weeks postsurgery (Faxitron MX-20 Digital, Tucson, AZ, USA). Images were anonymized and scored by three blinded reviewers (LBP, M-TAL, CE) as 1 for bridged and 0 for not bridged, and average scores > 0.66 (two of three blinded reviewers concurring) were considered bridged. Micro-CT (Viva-CT 40; Scanco Medical, Wayne, PA, USA) was performed on anesthetized animals for all time points, and three-dimensional image reconstructions were used to quantify bone formation with a mineral density threshold of $> 50\%$ of native bone designated as new bone, as described earlier [16, 34]. The central 121 image slices corresponding to approximately the central 4.6 mm of the defect length were analyzed for differences. BV and BD across the two treatment groups and time points were calculated for statistical comparisons ($n = 14$ per group) as described previously [8, 27, 34]. To accurately quantify the amount of new bone formation in the presence of mature autograft material, the respective 2-week BVs were used as a baseline to subtract from the subsequent volumes for each sample.

Histological Analyses

Vital Bone Labels

Two animals were administered a series of bone labels: calcein green (10 mg/kg; Sigma C0875) at 4 weeks, xylenol orange (100 mg/kg; Sigma 398187) at 8 weeks, and calcein blue (10 mg/kg; Sigma M1255) at 12 weeks postsurgery as subcutaneous injections to identify temporal mineralization patterns [15, 29, 33, 42]. Fixed samples were processed into cryoblocks, and nondecalcified sections (5 µm) were obtained to qualitatively observe repair, the mineral deposition pattern visualized by bone labels, and alkaline phosphatase (AP) staining for osteoblastic activity [21, 22, 41, 44]. Slides were imaged at × 5 magnification and high-resolution image mosaics were acquired.

Routine Histology

Samples for histological analyses were harvested at 2, 4, 6, 8, and 12 weeks postsurgery ($n = 1$–2), fixed, cleared of excess soft tissue around the defect, decalcified in formic acid (Cal-ExII; Fisher Scientific), and paraffin-embedded. Five-micron sagittal sections were cut and stained with hematoxylin and eosin (H&E), Safranin-O and Fast green [34], Mallory's aniline blue [40], and Picrosirius red stain [34] to qualitatively determine the progression of mineralization, the presence of cartilage, and the degree of mineralization of the bony structures within the healing defect, respectively.

Biomechanical Testing

Torsional testing was used as the index of functional recovery of the bone. Torsional tests to failure were performed on samples harvested at 12 weeks postsurgery (n = 9 per treatment group) as established earlier [8, 27, 28, 34]. Frozen samples were thawed at room temperature, dissected to remove all soft tissues surrounding the defects, and then the fixation plates were removed. The disarticulated bone ends were potted in Wood's metal (Alfa Aesar, Ward Hill, MA, USA) and tested to failure in torsion (Bose ELF 3200, 3° per second axial rotation in one direction irrespective of femur tested). Samples were covered in saline gauze after dissection until testing. The torque-rotation curve was used to calculate the maximum torque and torsional stiffness (slope of the linear region) for each sample [31].

Statistical Analysis

Differences in BV and BD over time were examined in a repeated-measures two-way analysis of variance model with significance set at $\alpha = 0.05$ (GraphPad; Prism, La Jolla, CA, USA) with post hoc comparisons for pairwise differences. Differences in biomechanical test parameters (maximum torque and torsional stiffness) were evaluated by a Student's t-test or its nonparametric equivalent, the Mann-Whitney U-test. Data are presented as mean ± SD.

Results

Comparison of Defect Mineralization and Morphology Over Time Between NMA-rhBMP-2 and Autograft Treatments

Overall, the NMA-rhBMP-2 group showed higher total BV, higher new BV, and lower BD compared with the autograft group by 12 weeks.

Defect Bridging

Radiographs qualitatively showed progressive mineralization from 4 to 12 weeks in the NMA-rhBMP-2 groups (Fig. 2A) and suggested more dense bone in the autograft-treated defects. Defect bridging was observed in 11 of 15 autografts and 14 of 15 NMA-rhBMP-2 samples at 12 weeks (Table 1).

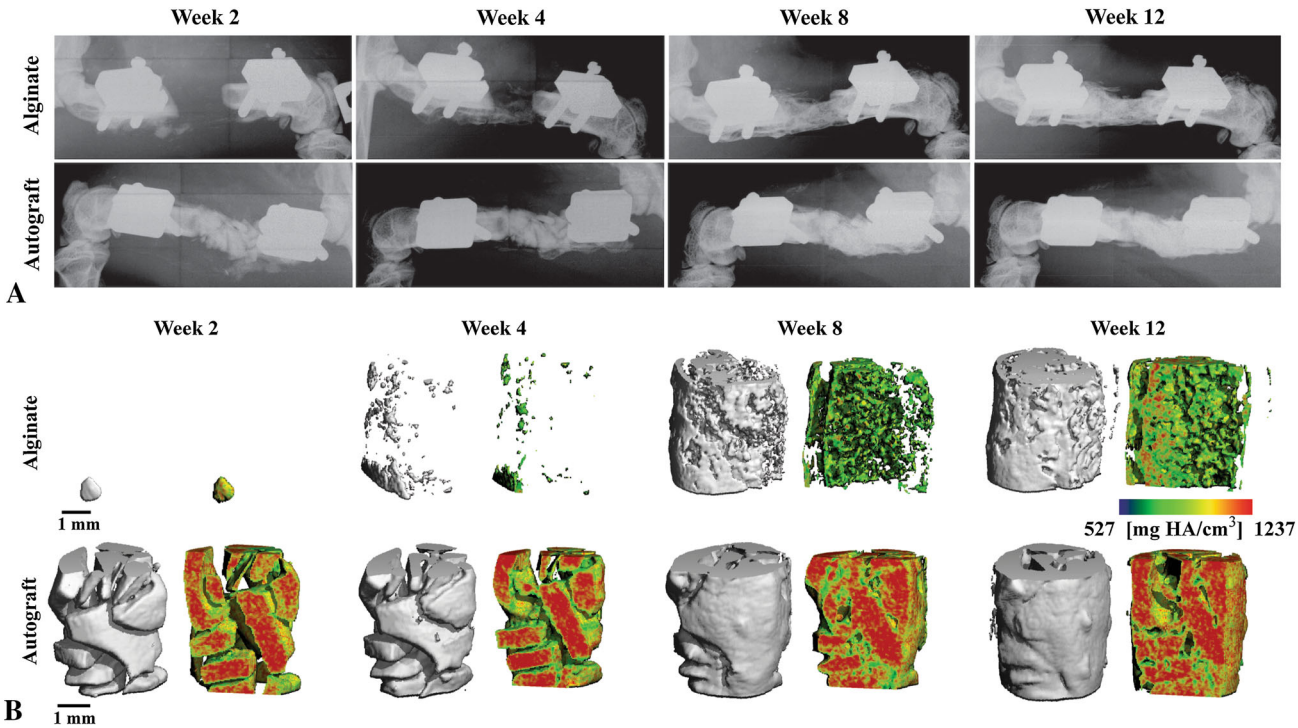

Fig. 2A–B Representative radiographs (**A**) and micro-CT reconstructions (**B**) show a defect bridging over time in the two treatment groups. The autograft showed radiodense shadows around bone fragments as early as 2 weeks suggesting early mineralization. The NMA-rhBMP-2 group only showed limited bone formation at the early time points (2, 4 weeks). The analyzed midsection of the defects is shown with an overlay of the bone mineral density map (color map scale: 527–1237 mg HA/cm^3).

Table 1. Bridging scores between the two groups over time determined from blinded scoring of radiographs showed apparent early healing of autograft but better bridging at 12 weeks for the NMA-rhBMP-2 group

Treatment groups	Radiographic bridging with time			
	2 weeks	4 weeks	8 weeks	12 weeks
NMA-rhBMP-2	0/22	0/21	14/18	14/15
Autograft	4/22	4/21	14/18	11/15

NMA-rhBMP-2 = nanofiber mesh alginate–recombinant human bone morphogenetic protein-2.

Bone Mineral Volume

Micro-CT analysis showed a similar progression of mineralization (Fig. 2B). The total BVs were 3.01 ± 2.34, 17.22 ± 10.37, 57.91 ± 16.73, and 75.60 ± 18.86 mm^3 ($n = 14$) at 2, 4, 8, and 12 weeks, respectively, in the NMA-rhBMP-2 group and 40.75 ± 3.98, 45.90 ± 6.45, 51.94 ± 10.58, and 55.40 ± 12.45 mm^3 ($n = 14$) at 2, 4, 8, and 12 weeks, respectively, in the autograft-treated group. BV in autograft-treated defects, which included both the implanted autograft bone and newly formed bone, was higher than that measured for the NMA-rhBMP-2 group at 2 and 4 weeks ($p < 0.001$). However, by 8 weeks (dotted line, Fig. 3A), there was no difference between the treatment groups. Notably, by 12 weeks, total BV was higher in the NMA-rhBMP-2 group ($p < 0.001$). Within groups, BV in the NMA-rhBMP-2 group increased over time ($p < 0.001$; Fig. 3A). BV increases were less marked in the autograft group with differences only observed at 12 weeks (from 2- and 4-week levels, $p < 0.05$) and at 8 weeks (from the 2-week level, $p < 0.001$). The volume of newly formed bone was higher for the NMA-rhBMP-2 group (54.90 ± 16.14, 72.59 ± 18.34 mm^3 [$n = 14$]; 8 and 12 weeks) compared with autograft treatment (11.19 ± 8.59, 14.64 ± 10.36 mm^3 [$n = 14$]; 8 and 12 weeks) at both 8 and 12 weeks (Fig. 3B: a, b; $p < 0.001$). Within groups, this new bone volume increased at all time points for the NMA-rhBMP-2 treatment group ($p < 0.001$), whereas the autograft group leveled off at 8 weeks ($p < 0.05$; Fig. 3B).

Bone Mineral Density

BD in the NMA-rhBMP-2 group remained lower than autograft at all time points (Fig. 4; $p < 0.001$). The BD values were 524.55 ± 47.25, 571.47 ± 34.99, 684.97 ± 25.07, and 779.96 ± 21.72 mm HA/ cm^3 ($n = 14$) at 2, 4, 8, and 12 weeks, respectively, in the NMA-rhBMP-2 group and 937.22 ± 36.95, 930.86 ± 39.48, 964.30 ± 32.77, and 1000.48 ± 23.15 mm HA/ cm^3 ($n = 14$) at 2, 4, 8, and 12 weeks, respectively, in the autograft-treated group. BD in the NMA-rhBMP-2 treatment group increased over time ($p < 0.001$, for comparisons between incremental times, eg, 2–4, 4–8, 8–12), but BD increases in the autograft group were noted only at 8 and 12 weeks compared with preceding levels ($p < 0.05$).

Defect Morphology and Mineralization Pattern

Stark qualitative differences in distribution of newly deposited mineral were noted between the two groups on examination of vital bone stain labeled samples as well as by routine histological staining (Fig. 5A–B) and representative images are presented in the following sections (Figs. 5–7).

Vital Bone Stains

In the NMA-rhBMP-2 group, green (calcein) and red (xylenol) labels administered at 4 and 8 weeks, respectively, were diffusely distributed (Fig. 5C), whereas the autograft group showed localized mineral deposition at the graft edges and in focal areas within the grafts at 4 weeks (green) followed by predominantly edge deposition at 8 weeks (red) (Fig. 5D). Although the calcein blue label, administered as a vital label subcutaneously (12 weeks), was not clearly visualized, continued mineralization at 12 weeks was evident in both groups by subsequent calcein blue staining of the sections (Fig. 5E–F). AP activity was diffusely distributed in the defect (Fig. 5G) in the NMA-rhBMP-2 group, but only limited, edge-localized activity (Fig. 5H) was evident in the autograft group. Overall, vital bone labels suggested a more localized region of new bone formation in the autograft group compared with the NMA-rhBMP-2 group (Fig. 5I–J).

Routine Histology

The NMA-rhBMP-2 group showed progressive mineralization (eosin-pink) and residual alginate (hematoxylin-purple) with time in H&E-stained sections (Fig. 6A–D). Safranin-O stain confirmed this mineral and alginate

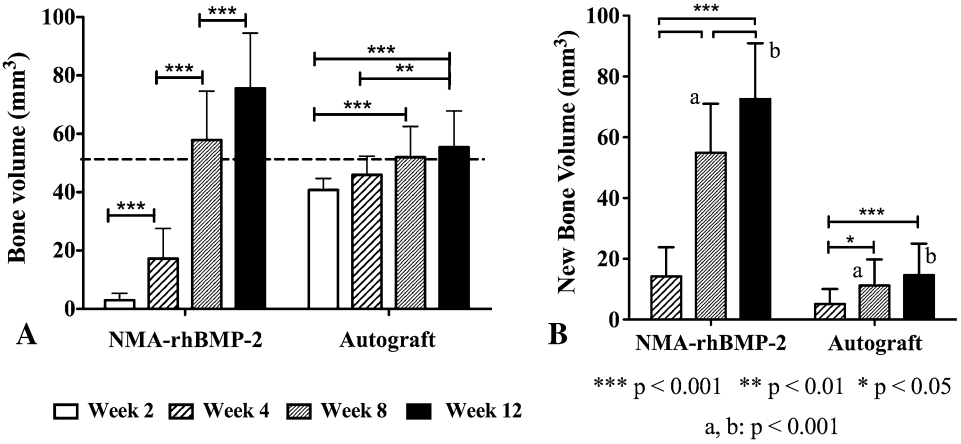

Fig. 3A–B Comparison of BV between the two groups with time is shown. (**A**) Total BV increased significantly in the NMA-rhBMP-2 group with time. This increase was much less marked in the autograft group. The dotted line represents the mean BV of autograft group at 8 weeks. The NMA-rhBMP-2 BV was significantly lower than the autograft group earlier than 8 weeks and was significantly higher subsequently ($p < 0.05$). (**B**) Comparing only the new bone formed beyond 2 weeks (subtraction of 2-week values) revealed the significantly lower new bone formation in the autograft group compared with the NMA-rhBMP-2 group at 8 and 12 weeks (a, b: $p < 0.001$). Within each group, however, the new BV rose significantly over time.

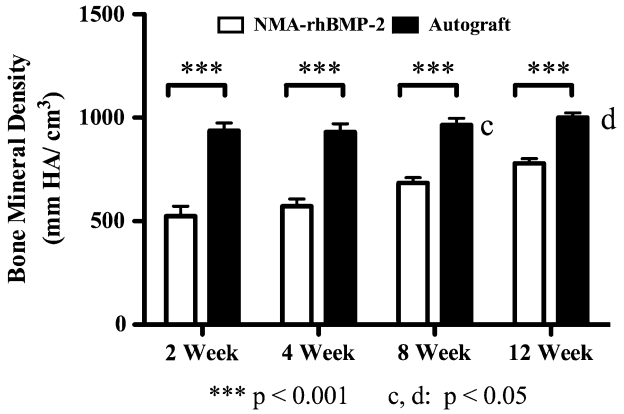

Fig. 4 Comparison of bone mineral density (BMD) between groups with time. Bone density in the NMA-rhBMP-2 group was always lower than that of autograft ($p < 0.001$). The mineral density increased significantly with time within both groups ($p < 0.05$) but was less marked in the autografts (Autograft: c, d = higher than the preceding time points within the group, NMA-rhBMP-2: all increments with time, $p < 0.001$) (mean ± SD; n = 14).

distribution (bone and connective tissue: blue; alginate and cartilage: red/orange; Fig. 6E–H). Mallory's aniline blue staining revealed mature bone formation (red) with time and smaller pieces of disintegrating alginate hydrogel (blue, acellular; Fig. 6I–L). Cartilage tissue was not readily apparent in this group, although regions of marrow formation were evident. Picrosirius red stain under polarized light revealed more red/green birefringent areas (more organized tissue) with time indicating a degree of remodeling to fibrolamellar bone (Fig. 6M–P).

Autograft-treated defects showed minimal surface appositional bone growth at 2 weeks by H&E stain, progressing to union between autograft fragments by 4 weeks and overall union between autograft pieces by 12 weeks (Fig. 7A–D). Safranin-O stain confirmed this observation and showed only sporadic areas of cartilage between graft fragments at early time points (Fig. 7E–H). Mallory's aniline blue stain confirmed the presence of sporadic cartilage areas between the autograft pieces and revealed mature bone stained deep red at 8 and 12 weeks (Fig. 7I–L). The new bone was localized primarily at the edges of the cortical graft, but Picrosirius stain revealed birefringent areas suggestive of lamellar bone at graft edges (Fig. 7M–P). Sporadic areas of cartilage were noted between graft fragments (Fig. 7B, F, J) and fibrous union between some autograft pieces was observed. Mature bone between autograft pieces was observed at 8 and 12 weeks.

Biomechanical Testing

The maximum torque at failure was 0.270 ± 0.108 and 0.125 ± 0.137 N-m and the torsional stiffness was 0.042 ± 0.019 and 0.020 ± 0.022 N-m/° for the NMA-rhBMP-2 group and the autograft group, respectively. The NMA-rhBMP-2-treated group revealed better functional regeneration with higher torsional stiffness ($p = 0.037$) and higher maximum torque ($p = 0.024$) compared with autograft (Fig. 8). The torque and stiffness values for the NMA-rhBMP-2-treated group corresponded well with

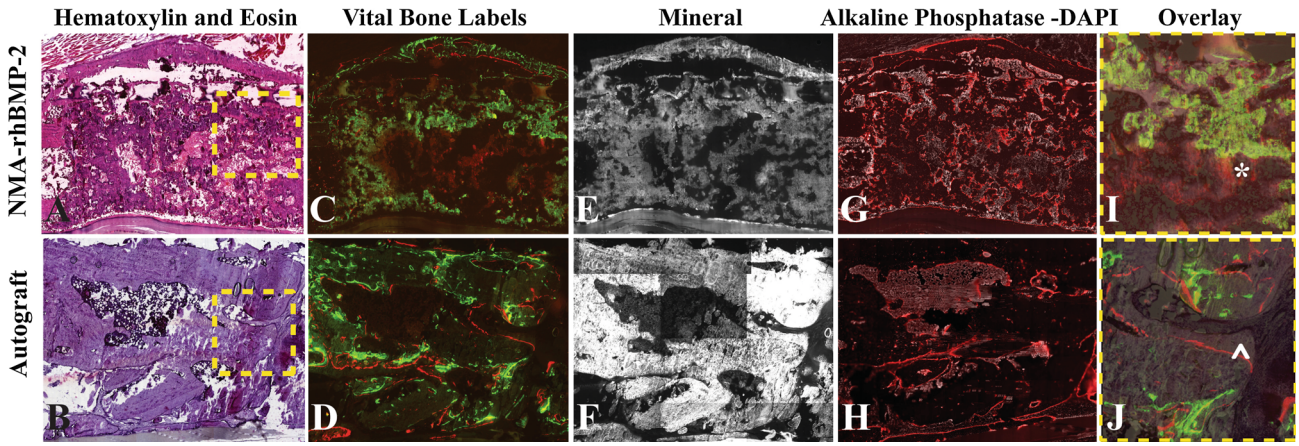

Fig. 5A–J Representative nondecalcified cryosections (5 µm) at 12 weeks were processed for routine H&E staining (**A**–**B**), vital bone labels (green = Week 4; red = Week 8) (**C**–**D**), mineral content (**E**–**F**), AP (osteoblastic activity) (**G**–**H**), and DAPI (nuclear) on the same sections. Images **I** and **J** are overlay images of the regions identified in **A** and **B**. The NMA-rhBMP-2 group showed diffuse mineral deposition in the defect at 4 weeks with evidence of continued activity (**A**, **C**, **E**, **I** [region of interest denoted by *]). Limited AP activity was also diffusely distributed in the defect and appeared at the mineralizing edge of the bone (**G**). The autograft group showed a more localized mineral deposition at the graft edges and focal areas within the grafts at 4 weeks followed by predominantly edge deposition at 8 weeks (**B**, **D**, **F**, **J** [region of interest denoted by ^]). Very limited AP activity was noted on some autograft margins and the defect boundary (**H**). (Composite images show entire defect in both cases [**A**–**H**]; magnification × 5).

previously reported values for this model and were comparable to the reported value of intact bone in the literature (dotted line in Fig. 8A–B) [8, 28].

Discussion

Autografts are the gold standard in the treatment of volumetric bone defects by virtue of their availability, compatibility, and high success rate despite inherent complications such as donor site morbidity. Although autograft provides scaffold, osteoinductive proteins, and osteogenic cells, challenges still exist in their use such as limited availability and associated morbidity [18]. Clinically, rhBMP-2 has been used to overcome the limitations of bone grafting such as slow healing and nonunion. Scaffold-based BMP delivery, especially on an absorbable collagen sponge (eg, ACS-rhBMP-2), has become popular as a clinical therapeutic alternative, at least in the United States, on the basis of promising animal and clinical results [20, 24, 35, 37, 38, 46]. However, evidence of large doses of rhBMP-2 leading to instances of heterotopic ossification, excessive inflammation, or poor bone structure has led to concerns regarding its clinical use, where an exact dose-response relationship has not been determined [6, 37, 38, 47]. It is thought that research that demonstrates efficacy with use of lower doses and/or a more sustained delivery of rhBMP-2 could thus lead to increased use of rhBMP-2 in place of autografts. We have previously demonstrated improved functional bone regeneration when directly comparing the NMA-rhBMP-2 hybrid delivery system with the ACS-rhBMP-2 delivery system for the same dose of rhBMP-2 [8, 27]. However, the efficacy of the NMA-rhBMP-2 hybrid delivery system has never been compared with use of live autograft to augment healing of critically sized long bone segmental defects. In this study, we demonstrate that NMA-rhBMP-2 treatment provides improved bone regeneration and restoration of biomechanical function compared with morselized cortical autograft treatment in a rat model.

This study used morselized cortical autograft to fill the critically sized segmental defect. A nonhomogenous size distribution of the autograft pieces was used here. Although some have shown that using highly morselized autograft fragments of cortical bone (25 µm to 2 mm, in canines) resulted in fibrous nonunion [23], benefits of smaller bone fragments have also been reported, likely arising from larger surface area [13] or better distribution of available periosteal or endosteal cells [26]. Typically, cortical autograft is gradually remodeled and replaced by regenerating bone, often delaying healing [11, 12, 19]. It is conceivable that use of cancellous autograft fragments may have produced better mineralization and functional recovery than observed in this study. However, the large volume of autologous cancellous bone that would have been required to fill the large defect in this preclinical study, like in actual clinical practice, precluded its use as a result of limited availability. Regardless of the source of autograft, the results of this study and earlier work [37] support that a comparable and even improved degree of healing can be

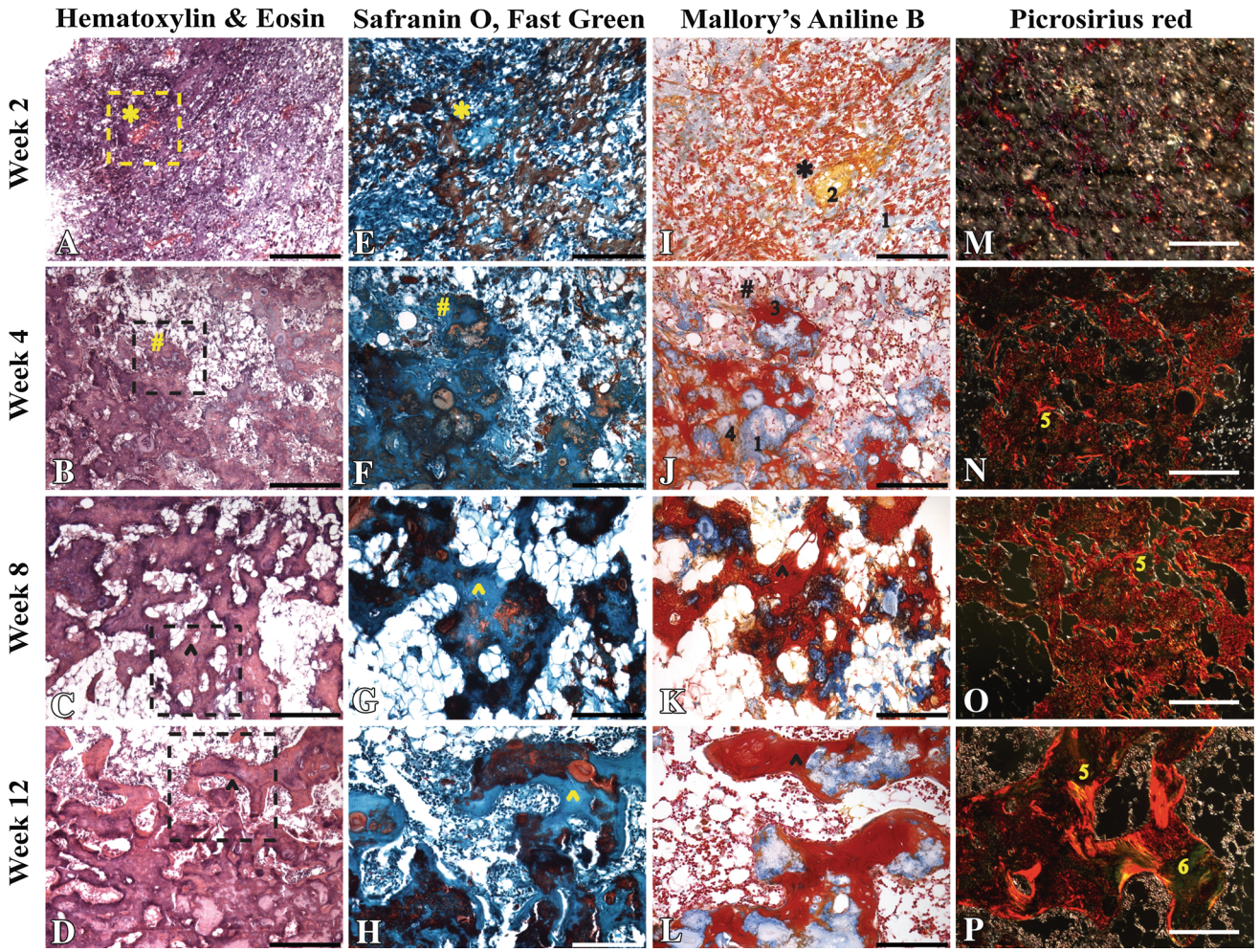

Fig. 6A–P Representative decalcified paraffin sections (5 μm) of NMA-rhBMP-2 samples at 2 to 12 weeks were processed for routine H&E staining (**A–D**), Safranin-O/Fast green (**E–H**), Mallory's modified aniline blue stain (**I–L**), and Picrosirius red (**M–P**) staining to characterize bone regeneration. Dotted lines in H&E images indicate areas of higher magnification shown in Safranin-O or Mallory's stain images, whereas Picrosirius stain images are from nonoverlapping areas. Bone appeared pink in H&E sections (**A–D**), whereas alginate and partly mineralized areas appeared pink-purple. Cartilage and alginate stained red with Safranin-O (**E–H**) and blue with Mallory's aniline stain (**I–L**). Additionally, mature bone stained deep red, whereas newly formed bone stained orange-red with Mallory's stain. Organized collagen structures, typical of mature bone, appeared brightly birefringent orange-red, yellow, or green with Picrosirius red stain under polarized light (**M–P**). Limited early bone formation was evident at 2 weeks (region of interest denoted by *) seen as pink areas (**A**), blue with Safranin-O (**E**), and orange-yellow with Mallory's (**I**, region of interest denoted by "2") and limited red staining areas with Picrosirius stain (**M**). Alginate appeared red in the Safranin-O-stained image and blue in Mallory's (**I**, region of interest denoted by "1"). Progressively more bone deposition was evident with time appearing as better-defined pink regions in H&E-stained sections (**A–D**). Corresponding sections stained with Safranin-O (**E–H**) showed blue areas of bone and red areas of remaining alginate. Mallory's stain with time (**I–L**) revealed an increase in deep red staining showing larger regions of mature bone (regions of interest denoted by ^ or "3") with less of poorly mineralized tissue–orange stain (**J** region of interest denoted by "4") and less residual alginate (1). Picrosirius red staining revealed increase in areas of birefringence with time suggestive of more fibrolamellar bone (regions of interest denoted by "5, 6" in **N–P**) (Scale: **A–D**: 300 μm, **E–P**: 150 μm).

achieved using the NMA-rhBMP-2 hybrid delivery system. Although a single dose of rhBMP-2 was evaluated in this study, its selection was based on a broader dose-effect study in this model comparing the NMA-rhBMP-2 hybrid delivery system and the ACS-rhBMP-2 system [8]. Lower doses of rhBMP-2 were used than are clinically prevalent, if one extrapolates from the clinical situation to the rat [8, 27]. Although qualitative radiographic assessments were made in our study, the use of micro-CT data provided better longitudinal and quantitative comparisons within and between groups. Furthermore, our reliance on torsional biomechanical testing as an assay of functional regeneration is a clinically relevant and widely accepted functional outcome measure. Finally, there is always a possibility of a systemic interaction between bilateral segmental defect surgeries, which may influence healing of

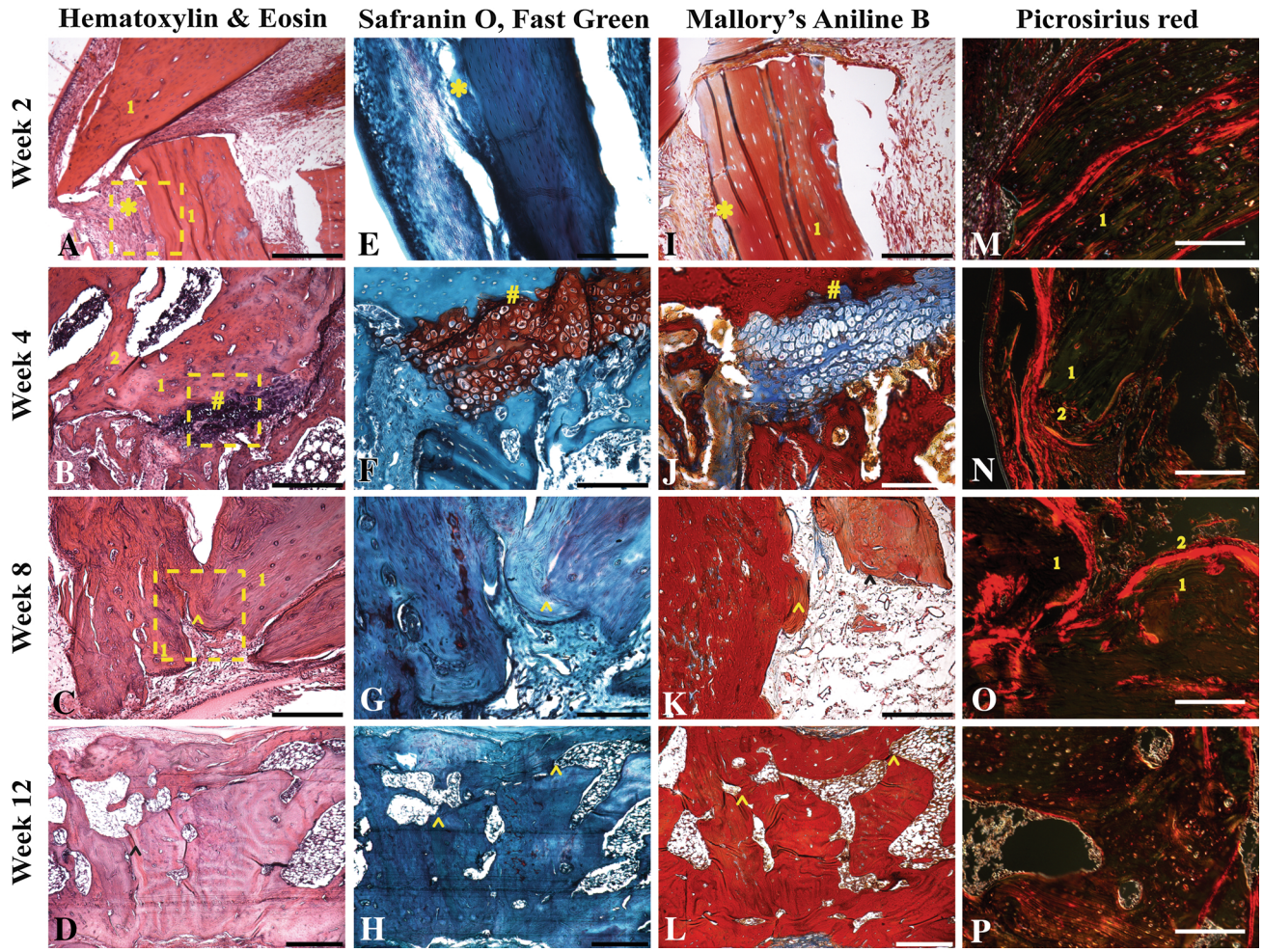

Fig. 7A–P Representative decalcified paraffin sections (5 μm) of the autograft group at 2 to 12 weeks were processed for routine H&E staining (**A–D**), Safranin-O (**E–H**), Mallory's aniline blue stain (**I–L**), and Picrosirius red (**M–P**) staining to characterize bone regeneration as with the NMA-rhBMP-2 group. The dotted lines in H&E images indicate areas magnified for corresponding image areas in Safranin-O and Mallory's aniline-stained sections (except **K**). Picrosirius red images are of nonoverlapping representative areas. The autograft group did not reveal clear evidence of appositional bone formation at 2 weeks by H&E (**A**, 1). However, small focal areas showing a mix of endochondral and fibrolamellar appositional bone formation were visible on autograft surfaces (**A**, *). Safranin-O staining did not reveal clear cartilage areas (**E**, *), but blue staining regions were evident with Mallory's stain with areas of new immature bone deposition (**I**, *). Picrosirius stain confirmed this early mineralization near the bone stump with minimal activity in the autograft pieces (**M**, 1). At 4 weeks, cartilage (**B**, #) was clearly visible in a focal region between autograft fragments (**B**, 1) and more mature appositional bone at the autograft margins (**B**, 2). Red staining of corresponding areas of cartilage with Safranin-O (**F**, #) and blue cartilage (#) and red adjacent bone in Mallory's stain confirmed the presence of cartilage and more mature appositional bone, respectively (**J**). Picrosirius stain revealed organized fiber structures with stark birefringence (**N**, 2) at the autograft edges (**N**, 1). At 8 weeks, appositional mineralized connections (**C**, ^) between autograft pieces were clearly visible (**C**, 1). This area did not stain for cartilage (**G**, ^), but core areas of red staining suggestive of cartilage were visible in the autografts with Safranin-O stain (**G**). In other areas, varying amounts of new bone mainly on the surface of autograft-appositional bone were visible (**K**, ^) without staining for cartilage tissue. Picrosirius staining confirmed this surface localization with brightly birefringent areas (**O**, 2) along autograft (**O**, 1) margins. At 12 weeks, the autograft pieces had progressed to bony union between autografts (^ in **D**, **H**, **L**) with Picrosirius staining showing typical organized structures in red-green birefringence (**P**) (Scale: **A**, **B**, **C** = 300 μm; **D**, **H**, **L** = 600 μm; others = 150 μm).

the respective individual defects. However, we have previously observed no interactive effects on bone healing even with high BMP delivery on one side. Differential weightbearing is another possible concern with bilateral surgery. However, this concern is minimized by the fact that even untreated defects are sufficiently stabilized by the fixation plates to allow excellent mobility a few days postsurgery [8, 14, 27, 28, 34].

Radiological bridging was observed in 93% of the NMA-rhBMP-2-treated defects and 73% of autograft-treated defects at 12 weeks. These data are consistent with previous studies showing 20% to 30% occurrence of

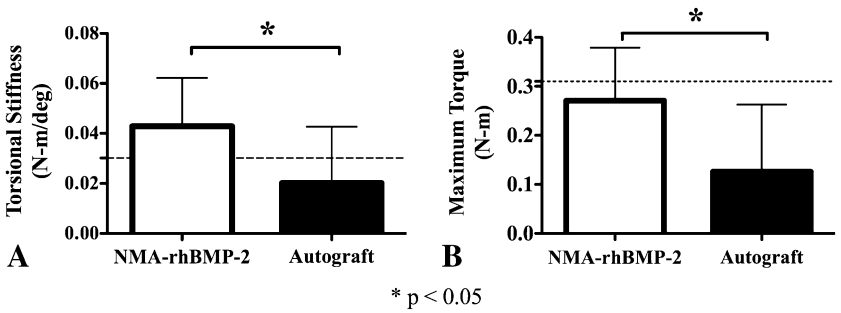

Fig. 8A–B Evaluation of functional regeneration as indicated by biomechanical properties is demonstrated. (**A**) Torsional testing showed a higher torsional stiffness in the NMA-rhBMP-2 group compared with the autograft group (*p = 0.037). (**B**) Maximum torque at failure was also higher for the NMA-rhBMP-2 group compared with autograft (*p = 0.02). The dotted line on both graphs represents the mean value for intact bone from literature [28, 34] (mean ± SD; n = 9).

nonunion or other complications like pseudoarthroses and graft fractures with cortical autograft [7, 17, 30]. The higher bridging rate observed for the NMA-rhBMP-2 group can be explained by the greater amount of new bone volume (over the 2-week levels) observed for this group compared with the autograft group. Although new BV (Fig. 3B) was not different between the two groups at 4 weeks, its distribution around the autograft fragments may have contributed to the appearance of early bridging in radiographs with autograft treatment. The autograft material, being typically radiodense, complicated interpretation of the micro-CT data and required us to subtract 2-week BV from subsequent values to obtain a better realization of newly formed bone in our longitudinal analysis. Furthermore, this comparison exposed the sharp contrast between the amounts of newly formed bone resulting from the two treatment strategies. The BD of the NMA-rhBMP-2 group was always lower than the autograft group but this was not surprising given that the autograft mineral density measurement reflected both the implanted bone graft and newly formed bone, whereas the NMA-rhBMP-2 group's mineral density was just newly formed bone. The autograft group BD also increased with time ($p < 0.05$, except between 2 and 4 weeks). For autograft, these findings are suggestive of limited osteoclastic activity and predominantly appositional bone formation. We did not observe an initial reduction in autograft density as previously reported [17]. This could be explained by the early appositional bone formation, which may limit osteoclast activity [26].

Vital bone labels clearly revealed that the mineralization in the NMA-rhBMP-2 group was more pronounced at the defect periphery initially but subsequently extended into the defect center. Conversely, the autograft displayed some areas of label (mineral) localization within the fragments at 4 weeks, but subsequent bone formation was largely limited to the periphery of the fragments. The presence of nuclei in the lacunae of the autograft suggested that the grafts retained viable cells that could participate in bone regeneration. In routine histology sections, the autograft group showed primarily appositional bone formation, mainly limited to their margins, at 4 weeks. Fibrovascular stroma [4] was observed around the autograft pieces in areas of limited healing. Although gene expression studies do not suggest endochondral healing as a primary mechanism of cortical autograft healing in rats [43], we observed small focal areas of cartilage, suggestive of endochondral ossification in the tissue between some autograft pieces at 4 weeks of healing in addition to the typical appositional intramembranous bone formation. This is likely explained by contributions from the graft-derived cells or by migration of stem cells/osteoprogenitor cells into the defect region, although this was not specifically characterized in this study. Although the diffusion-limited environment in large autografts may limit viability to only surface cells on the grafts [19], it is possible that the morselized nature of autograft used in this study contributed to mineralized healing either as a result of the larger available surface area or graft-associated cells [4, 5, 13, 26].

The NMA-rhBMP-2 group showed better mechanical properties at the 12-week time point despite the presence of some residual alginate [8, 28, 34]. Although reduced mechanical strength of cortical autograft has been reported during the early healing phase [11, 26], it is conceivable that the autograft group in this study could have progressed to improved mechanical strength with longer healing time. The large BV of comparable density formed in the NMA-rhBMP-2 group in this study underscores its potential as an effective alternative to current clinical interventions (eg, autograft, ACS-rhBMP-2 delivery systems) [8, 27]. Nevertheless, this treatment method was successful in inducing functional mineralized healing of a large segmental defect with maximum torque and torsional stiffness reaching the level of intact bone [28].

In conclusion, this study provides evidence that the NMA-rhBMP2 hybrid delivery system could be an

effective alternative to autograft treatment for repair of segmental bone defects. Future large animal preclinical studies are needed to confirm the efficacy of this approach and as a next step toward clinical translation.

Acknowledgments We thank Jason Wang, Ashley Allen, Angela Lin, Nick Servies, Sukhita Karthikeyakannan, and Kalah Haley for assistance with surgeries and sample processing.

References

1. Albert A, Leemrijse T, Druez V, Delloye C, Cornu O. Are bone autografts still necessary in 2006? A three-year retrospective study of bone grafting. *Acta Orthop Belg.* 2006;72:734–740.
2. Alsberg E, Anderson KW, Albeiruti A, Franceschi RT, Mooney DJ. Cell-interactive alginate hydrogels for bone tissue engineering. *J Dent Res.* 2001;80:2025–2029.
3. Alsberg E, Kong HJ, Hirano Y, Smith MK, Albeiruti A, Mooney DJ. Regulating Bone formation via controlled scaffold degradation. *J Dent Res.* 2003;82:903–908.
4. Anderson KJ. The behavior of autogenous and homogenous bone transplants in the anterior chamber of the rat's eye. A histological study of the effect of the size of the implant. *J Bone Joint Surg Am.* 1961;43:980–995.
5. Anderson KJ, Schmidt J, Lecocq JF. The effect of particle size of the heterogenous-bone transplant on the host-tissue vascular penetration. *J Bone Joint Surg Am.* 1959;41:1455–1468.
6. Angle SR, Sena K, Sumner DR, Virkus WW, Virdi AS. Healing of rat femoral segmental defect with bone morphogenetic protein-2: a dose response study. *J Musculoskelet Neuronal Interact.* 2012;12:28–37.
7. Basarir K, Selek H, Yildiz Y, Saglik Y. [Nonvascularized fibular grafts in the reconstruction of bone defects in orthopedic oncology] [in Turkish]. *Acta Orthop Traumatol Turc.* 2005;39:300–306.
8. Boerckel JD, Kolambkar YM, Dupont KM, Uhrig BA, Phelps EA, Stevens HY, Garcia AJ, Guldberg RE. Effects of protein dose and delivery system on BMP-mediated bone regeneration. *Biomaterials.* 2011;32:5241–5251.
9. Boerckel JD, Kolambkar YM, Stevens HY, Lin AS, Dupont KM, Guldberg RE. Effects of in vivo mechanical loading on large bone defect regeneration. *J Orthop Res.* 2012;30:1067–1075.
10. Boerckel JD, Uhrig BA, Willett NJ, Huebsch N, Guldberg RE. Mechanical regulation of vascular growth and tissue regeneration in vivo. *Proc Natl Acad Sci U S A.* 2011;108:E674–680.
11. Burchardt H. Biology of cortical bone graft incorporation. In: Aebi M, Regazzoni P, eds. *Bone Transplantation.* New York, NY, USA: Springer; 1989:23–28.
12. Burwell RG. The function of bone marrow in the incorporation of a bone graft. *Clin Orthop Relat Res.* 1985;200:125–141.
13. Delloye C, Simon P, Nyssen-Behets C, Banse X, Bresler F, Schmitt D. Perforations of cortical bone allografts improve their incorporation. *Clin Orthop Relat Res.* 2002;396:240–247.
14. Dosier CR, Uhrig BA, Willett NJ, Krishnan L, Li MT, Stevens HY, Schwartz Z, Boyan BD, Guldberg RE. Effect of cell origin and timing of delivery for stem cell-based bone tissue engineering using biologically functionalized hydrogels. *Tissue Eng A.* 2015;21:156–165.
15. Du SJ, Frenkel V, Kindschi G, Zohar Y. Visualizing normal and defective bone development in zebrafish embryos using the fluorescent chromophore calcein. *Dev Biol.* 2001;238:239–246.
16. Duvall CL, Taylor WR, Weiss D, Wojtowicz AM, Guldberg RE. Impaired angiogenesis, early callus formation, and late stage remodeling in fracture healing of osteopontin-deficient mice. *J Bone Miner Res.* 2007;22:286–297.
17. Enneking WF, Eady JL, Burchardt H. Autogenous cortical bone grafts in the reconstruction of segmental skeletal defects. *J Bone Joint Surg Am.* 1980;62:1039–1058.
18. Finkemeier CG. Bone-grafting and bone-graft substitutes. *J Bone Joint Surg Am.* 2002;84:454–464.
19. Goldberg VM. Natural history of autografts and allografts. In: Older MWJ, ed. *Bone Implant Grafting*. London, UK: Springer-Verlag; 1992:9–12.
20. Govender S, Csimma C, Genant HK, Valentin-Opran A, Amit Y, Arbel R, Aro H, Atar D, Bishay M, Borner MG, Chiron P, Choong P, Cinats J, Courtenay B, Feibel R, Geulette B, Gravel C, Haas N, Raschke M, Hammacher E, van der Velde D, Hardy P, Holt M, Josten C, Ketterl RL, Lindeque B, Lob G, Mathevon H, McCoy G, Marsh D, Miller R, Munting E, Oevre S, Nordsletten L, Patel A, Pohl A, Rennie W, Reynders P, Rommens PM, Rondia J, Rossouw WC, Daneel PJ, Ruff S, Ruter A, Santavirta S, Schildhauer TA, Gekle C, Schnettler R, Segal D, Seiler H, Snowdowne RB, Stapert J, Taglang G, Verdonk R, Vogels L, Weckbach A, Wentzensen A, Wisniewski T. Recombinant human bone morphogenetic protein-2 for treatment of open tibial fractures: a prospective, controlled, randomized study of four hundred and fifty patients. *J Bone Joint Surg Am.* 2002;84:2123–2134.
21. Hong SH, Jiang X, Chen L, Josh P, Shin DG, Rowe D. Computer-automated static, dynamic and cellular bone histomorphometry. *J Tissue Sci Eng.* 2012;Suppl 1:004.
22. Jiang X, Kalajzic Z, Maye P, Braut A, Bellizzi J, Mina M, Rowe DW. Histological analysis of GFP expression in murine bone. *J Histochem Cytochem.* 2005;53:593–602.
23. Johnson KD, August A, Sciadini MF, Smith C. Evaluation of ground cortical autograft as a bone graft material in a new canine bilateral segmental long bone defect model. *J Orthop Trauma.* 1996;10:28–36.
24. Jones AL, Bucholz RW, Bosse MJ, Mirza SK, Lyon TR, Webb LX, Pollak AN, Golden JD, Valentin-Opran A; BMP-2 Evaluation in Surgery for Tibial Trauma-Allograft (BESTT-ALL) Study Group. Recombinant human BMP-2 and allograft compared with autogenous bone graft for reconstruction of diaphyseal tibial fractures with cortical defects. A randomized, controlled trial. *J Bone Joint Surg Am.* 2006;88:1431–1441.
25. Jones CB, Sabatino CT, Badura JM, Sietsema DL, Marotta JS. Improved healing efficacy in canine ulnar segmental defects with increasing recombinant human bone morphogenetic protein-2/allograft ratios. *J Orthop Trauma.* 2008;22:550–559.
26. Khan SN, Cammisa FP Jr, Sandhu HS, Diwan AD, Girardi FP, Lane JM. The biology of bone grafting. *J Am Acad Orthop Surg.* 2005;13:77–86.
27. Kolambkar YM, Boerckel JD, Dupont KM, Bajin M, Huebsch N, Mooney DJ, Hutmacher DW, Guldberg RE. Spatiotemporal delivery of bone morphogenetic protein enhances functional repair of segmental bone defects. *Bone.* 2011;49:485–492.
28. Kolambkar YM, Dupont KM, Boerckel JD, Huebsch N, Mooney DJ, Hutmacher DW, Guldberg RE. An alginate-based hybrid system for growth factor delivery in the functional repair of large bone defects. *Biomaterials.* 2011;32:65–74.
29. Konig Junior B, Beck TJ, Kappert HF, Kappert CC, Masuko TS. A study of different calcification areas in newly formed bone 8 weeks after insertion of dental implants in rabbit tibias. *Ann Anat.* 1998;180:471–475.
30. Krieg AH, Hefti F. Reconstruction with non-vascularised fibular grafts after resection of bone tumours. *J Bone Joint Surg Br.* 2007;89:215–221.
31. Oest ME, Dupont KM, Kong HJ, Mooney DJ, Guldberg RE. Quantitative assessment of scaffold and growth factor-mediated

repair of critically sized bone defects. *J Orthop Res.* 2007;25:941–950.
32. Oryan A, Alidadi S, Moshiri A, Maffulli N. Bone regenerative medicine: classic options, novel strategies, and future directions. *J Orthop Surg Res.* 2014;9:18.
33. Pautke C, Vogt S, Tischer T, Wexel G, Deppe H, Milz S, Schieker M, Kolk A. Polychrome labeling of bone with seven different fluorochromes: enhancing fluorochrome discrimination by spectral image analysis. *Bone.* 2005;37:441–445.
34. Priddy LB, Chaudhuri O, Stevens HY, Krishnan L, Uhrig BA, Willett NJ, Guldberg RE. Oxidized alginate hydrogels for bone morphogenetic protein-2 delivery in long bone defects. *Acta Biomater.* 2014;10:4390–4399.
35. Reichert JC, Cipitria A, Epari DR, Saifzadeh S, Krishnakanth P, Berner A, Woodruff MA, Schell H, Mehta M, Schuetz MA, Duda GN, Hutmacher DW. A tissue engineering solution for segmental defect regeneration in load-bearing long bones. *Sci Transl Med.* 2012;4:141ra193.
36. Rowley JA, Madlambayan G, Mooney DJ. Alginate hydrogels as synthetic extracellular matrix materials. *Biomaterials.* 1999;20:45–53.
37. Sciadini MF, Johnson KD. Evaluation of recombinant human bone morphogenetic protein-2 as a bone-graft substitute in a canine segmental defect model. *J Orthop Res.* 2000;18:289–302.
38. Shields LB, Raque GH, Glassman SD, Campbell M, Vitaz T, Harpring J, Shields CB. Adverse effects associated with high-dose recombinant human bone morphogenetic protein-2 use in anterior cervical spine fusion. *Spine.* 2006;31:542–547.
39. Simmons CA, Alsberg E, Hsiong S, Kim WJ, Mooney DJ. Dual growth factor delivery and controlled scaffold degradation enhance in vivo bone formation by transplanted bone marrow stromal cells. *Bone.* 2004;35:562–569.
40. Sterchi D, Keefer L. Modified Mallory aniline blue stain for bone, cartilage, and other connective tissues. *J Histolotechnol.* 1998;21:129–133.
41. Ushiku C, Adams DJ, Jiang X, Wang L, Rowe DW. Long bone fracture repair in mice harboring GFP reporters for cells within the osteoblastic lineage. *J Orthop Res.* 2010;28:1338–1347.
42. van Gaalen SM, Kruyt MC, Geuze RE, de Bruijn JD, Alblas J, Dhert WJ. Use of fluorochrome labels in in vivo bone tissue engineering research. *Tissue Eng B Rev.* 2010;16:209–217.
43. Virolainen P, Vuorio E, Aro HT. Gene expression at graft-host interfaces of cortical bone allografts and autografts. *Clin Orthop Relat Res.* 1993;297:144–149.
44. Wang YH, Liu Y, Maye P, Rowe DW. Examination of mineralized nodule formation in living osteoblastic cultures using fluorescent dyes. *Biotechnol Prog.* 2006;22:1697–1701.
45. Younger EM, Chapman MW. Morbidity at bone graft donor sites. *J Orthop Trauma.* 1989;3:192–195.
46. Zabka AG, Pluhar GE, Edwards RB 3rd, Manley PA, Hayashi K, Heiner JP, Kalscheur VL, Seeherman HJ, Markel. Histomorphometric description of allograft bone remodeling and union in a canine segmental femoral defect model: a comparison of rhBMP-2, cancellous bone graft, and absorbable collagen sponge. *J Orthop Res.* 2001;19:318–327.
47. Zara JN, Siu RK, Zhang X, Shen J, Ngo R, Lee M, Li W, Chiang M, Chung J, Kwak J, Wu BM, Ting K, Soo C. High doses of bone morphogenetic protein 2 induce structurally abnormal bone and inflammation in vivo. *Tissue Eng A.* 2011;17:1389–1399.